Journal of Thermal Analysis and Calorimetry, Vol. 87 (2007) 2, 529–537

THERMAL MANAGEMENT FOR A POLY(METHYL ACRYLATE) OPTICAL FIBER IN SOLAR LIGHTING

M. Tekelioglu[1*] *and B. D. Wood*[2]

[1]Department of Mechanical Engineering, University of Nevada, Reno, NV 89557, USA
[2]Department of Mechanical and Aerospace Engineering, Utah State University, Logan, UT 84322, USA

We present a 3-D thermal analysis of a poly(methyl acrylate) optical fiber to select a method to prevent thermal degradation (TD) of the fiber. Such poly(methyl acrylate)-core optical fibers have been realized in many solar lighting applications. We give the radial and axial temperature distributions on the entrance region of the optical fiber for two solar collector designs and five different preventive methods. The simulation results showed that attachment of a fused quartz rod to the fiber entrance region was an efficient low-cost way to protect the optical fiber. A temperature was predicted for the deformed fiber entrance region of the experimental results from the simulations.

Keywords: *poly(methyl acrylate), solar lighting, thermal degradation*

Introduction

Plastic optical fibers (POFs) have been preferred in diverse applications from medical examination of internal organs to lighting of buildings and passenger cars. This is largely due to their low cost and high flexibility compared to silica-core fibers. These advantages come, however, in addition to their higher attenuation, with possible TD which can arise at a temperature as low as 60°C. TD, observable as a soft fiber core susceptible to any external damage may cause fiber aging, reduced life-time from years to months, and increased attenuation in the short visible region, λ=400–470 nm [1]. If thermal cycling occurs in the operation, e.g., from –20 to +30°C and back to –20°C, the core and clad of the fiber may not perfectly line up. Thus, for high-efficient and cost-effective operation of POFs, it is important to eliminate or reduce the adverse effects of TD.

A light distribution system was demonstrated in 1881 which was built from reflectively coated pipes, a light source, and diffusive output optics [2]. The authors concluded that lighting with fiber optics is expected to be competitive with conventional and high-performance lighting systems in terms of their lighting efficacy, life-time, and cost. Bandwidth and attenuation of the fibers were described [3]; effect of extrinsic factors on the optical fiber efficiency was included. The spectral (λ)-specular (φ) light loss coefficients for single skew and meridional rays were given on arbitrary straight optical fiber [4]. The authors compared their model results with available experimental data and found good agreement for rays that make a small angle of φ with the optical fiber axis (φ<20°). Radiative destruction by macromolecules was studied after addition of naphthalene and perdeuteronaphthalene into PMMA and PMMA-d8 (octa-deuteromethylmethacrylate) [5]. They used cobalt-60 γ-rays with a dose of 35 kGy (a dose rate of 2.5 Gy s^{-1} at 27°C). High optical losses observed in the absorption spectra λ=400–600 nm of PMMA-d8 was attributed to the formation of stable uncharged products in the case of perdeuteronaphthalene addition into PMMA-d8. POFs absorption over the visible spectrum was studied with vibrational and electronic absorption [6]. The former loss mechanism was due to stretching of the bonds between atoms, and the latter being due to transition electrons from the valence to the conduction band. The authors concluded that to minimize visible spectrum attenuation, the fiber core should have no N–H, O–H, or aliphatic C–H bonds in its repeat unit. In another paper, thermal stability and composition of the jute vinylester composite fibers were studied via alkaline treatment from chemical kinetics using thermogravimetry (TG) and differential TG curves [7]. Effect of heating on the fiber thermomechanical performance was investigated [8]. A double-jacket UV-cured acrylate fiber was used. The author observed a partial delamination of the jacket material between the primary and secondary coatings, at elevated temperatures, due to application of a cyclic force along the fiber axis. Effect of heating on the overall optical loss was studied [9]. They considered the fiber losses due to electronic absorption,

* Author for correspondence: tekeliog@unr.edu

1388–6150/$20.00

Akadémiai Kiadó, Budapest, Hungary
Springer, Dordrecht, The Netherlands

vibrational absorption, Rayleigh scattering, and structural impurities. Their measured results showed, before and after heating the fiber to 150°C, that electronic absorption caused the major increase in overall loss of the optical fiber. They attributed this to the small amount of conjugated carbonyls formed by a thermal oxidation reaction in the polymer core. In a gas reaction, 0.5 mm size poly(methyl methacrylate) optical fiber grains were used to determine the type of reaction (endothermic or exothermic) [10]. The author in that paper used TG/DTA/MS under O_2, N_2 and showed that the gas reaction was endothermic under inert environment and exothermic in oxidative environment (10% O_2 in N_2).

Experimental

Although the effect of heating on the optical and physical properties of select fibers has been studied, TD prevention has not received much attention. In this paper, we investigate ways to prevent or reduce the effect of TD. To do this, the fiber entrance region radial and axial temperature distributions were predicted from finite element analysis (FEA) for five different methods of filtering. A manufacturer's TD onset temperature of 60°C was used to evaluate the simulation results. The results predicted a temperature range for the fiber entrance region from the experimental data.

Solar lighting systems

In typical solar lighting systems, the solar visible spectrum λ=400–700 nm is transferred into luminaires via large-core polymer optical fibers. Several prototypes of such solar lighting systems have been made operational at the Oak Ridge Natural Laboratory (ORNL) [11].

Collector designs

TD of the PMA fiber was studied on two solar collector designs:

Eight-fiber design

In the design shown in Fig. 1a, the visible solar spectrum reflected from the primary and secondary mirrors enters eight individual fibers and gets subsequently transmitted into the luminaires. The amount of light on the fiber entrance region tip surface was ~8800 lumens measured with a spectrophotometer [11]. Lumen, a photometric term, is used to describe the quantity of light perceived by the photoreceptors, cones and rods, of the human eye [12].

Primary mirror is part of a paraboloid with a 118.1 cm outer diameter, 41.9 cm focal length, 30.5 cm borehole diameter, 0.64 cm thickness, and an estimated aperture area of 1 m^2. The mirror is made of a glass coated with enhanced aluminum by Flabeg Inc. The secondary mirror has eight planar segments each with a surface area of about 555 cm^2, a tilt angle of 25°C; the mirror is coated with silvered polymer by Navitar Coating Inc.

Fresnel lens design

The fresnel lens design utilizing a 88.9 cm fresnel lens and one single fiber is shown in Fig. 1b. Given the same optical properties of the primary and secondary mirrors and fresnel lens and excluding solar tracking and focal point accuracies, the lens design was estimated to transmit 3–4 times more lumens (light) per fiber compared to the previous design.

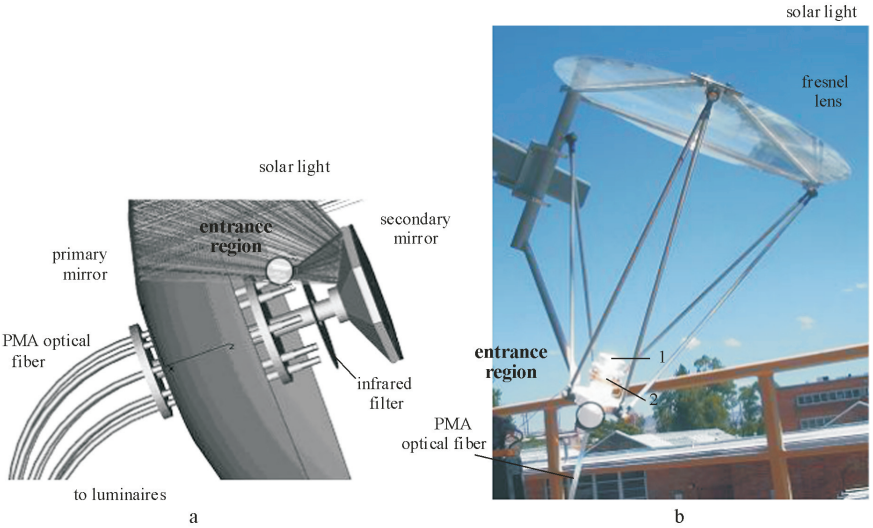

Fig. 1 a – Eight-fiber design, b – Fresnel lens design: 1 – hot mirror, 2 – infrared filter

FEA with ANSYS

We applied an FEA in TD study of the PMA-core fiber: Due to temperature dependent physical properties (ρ, c_p, and k) of the fiber core and clad materials, exact analytical solutions may not be readily found due to non-linearity of PDEs. Further, non-uniform profile of heat flux (irradiance, W m^{-2}) on the fiber entrance region tip surface of these designs was analytically difficult to translate and solve as a boundary condition problem. Additionally, the interactions at the fiber entrance region tip surface may involve other forms of heat transfer simultaneously, e.g., convection and radiation that precludes getting analytical solutions easily. Analytical solutions so-obtained may be a far estimate of the actual results. Nevertheless, non-linear PDEs with non-uniform heat flux input, and simultaneous heat transfer interactions at a boundary can be solved through FEA with sufficient accuracy. A relatively simpler finite difference analysis (FDA) was given on one optical fiber, which used Gaussian heat flux profile and constant physical properties for the fiber core and clad materials [13].

A model of atmosphere described in SMARTS [14] was used to predict the terrestrial direct normal solar spectral irradiance for air mass (*AM*=1.5) (Fig. 2). *AM* is the ratio of the mass of the air column at any time during the day to the mass of the air column at solar noon. *AM*=1.5 with an atmospheric turbidity of 0.27 is considered to be a year-round representative average atmosphere in the 48 contiguous states of the U.S. Heat flux profile of the solar infrared spectrum at the fiber entrance region tip surface was modeled and included from TracePro [15], a commercial raytrace software; a 3-D thermal FEA of the PMA-fiber was performed on ANSYS [16], combining the inputs of SMARTS and TracePro.

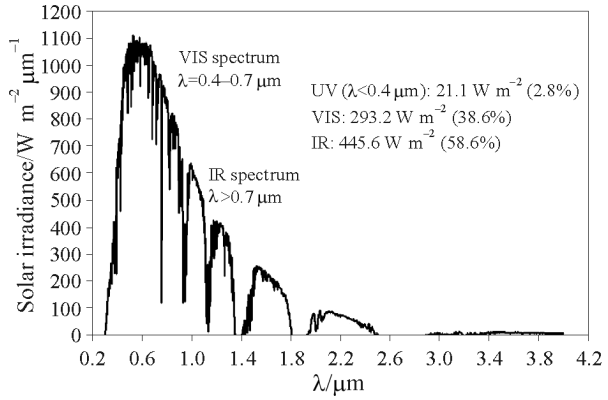

Fig. 2 Terrestrial direct normal solar spectral irradiance for *AM*=1.5 from [14]

Preventive methods

In the following, we give alternative solutions to TD prevention. We describe five methods to reduce the effect of TD: First method included the air-cooling of the fiber entrance region: The entrance region radial and axial temperature distributions were found for air velocity (v_∞) of 5, 10 and 15 m s^{-1}. Second method included the presence of an infrared filter or a hot mirror before the entrance region to reduce the amount of infrared heat flux. Third method investigated the attachment of a glass rod (vitreous silica-SiO_2 glass) to the fiber entrance region. This method was to reduce the direct heating effect of the infrared spectrum on the fiber entrance region through glass-rod internal heat storage and convective heat transfer between the rod and the surroundings. Fourth method implemented the coating of the fiber entrance region tip surface with a selective material, e.g. a white paint, having an emissivity (ε) of 0.6 or 0.8 in the infrared. The method aimed to augment the radiative heat transfer from the tip surface. Last, fifth, method investigated the effect of lower ambient temperature: T_∞=0 and –5°C were used in the simulations, T_∞=25°C (standard atmosphere).

Optical properties (hardware and fiber)

The optical reflectivity (*R*) of the primary and secondary mirrors and transmissivity (*T*) of the fresnel lens are shown in Fig. 3a. *R*-value of the primary mirror, hemispherical-directional [17], was measured with an integrating sphere. *R*-value of the secondary mirror was obtained from *T*-value of the mirror measured with 15% absorption (*A*-value) up to 0.4 μm and with 5% *A*-value between 0.4 and 2.5 μm. Average *R*-value of the secondary mirror over the visible was about 90%; *T*-value of the fresnel lens was measured with a spectrophotometer.

R and *T*-values for the infrared filter and hot mirror applied before the fiber entrance region are shown in Fig. 3b. The infrared filter absorbs the infrared solar spectrum and transmits the visible while the hot mirror reflects the infrared and transmits the visible. The infrared filter manufactured by Edmund Industrial optics had almost same average *T*-values for 0 and 45° incident angles with a slight shift realized for 45° incident angle centered nearly at 420 nm. Given an estimated maximum angle of about 28° for the incident rays, angle dependence of the infrared filter *T*-value was not considered.

Table 1 lists the basic information on the fiber core and clad materials. PMA optical fiber analyzed in this paper was constructed from a core transmitting the light and a lower refractive index clad ensuring light guiding and core protection. PMA-core fiber manufactured by 3M was cross-linked with a durabil-

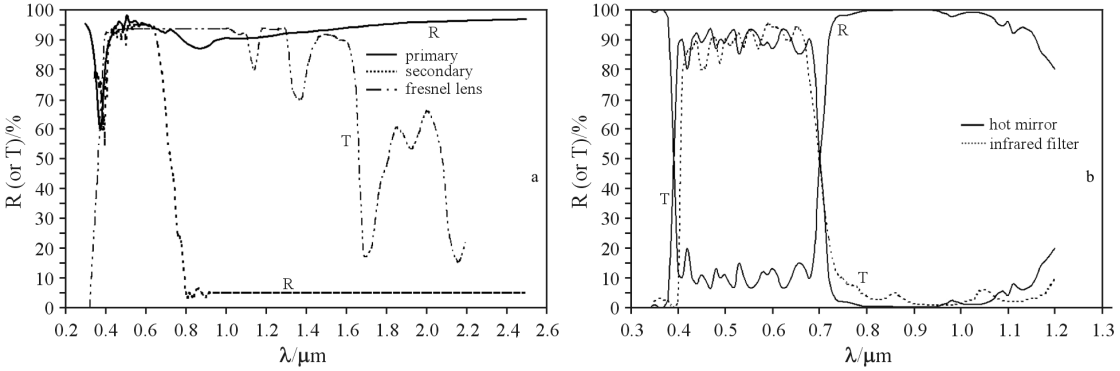

Fig. 3 a – *R*-value of the primary and secondary mirrors and *T*-value of the fresnel lens, b – *R*- and *T*-values of the infrared filter and hot mirror (T_∞=25°C)

ity of longer than 3 years for 60°C of operation. Temperature-dependent physical properties c_p, k and ρ of the PMA core and Teflon-FEP clad were taken from Brandrup [18] and Du-Pont [19], respectively. The glass rod (vitreous silica-SiO_2) physical properties were taken from Bansal [20].

Interactions at and inside the boundary

Heat flux

Heat flux input was of the infrared spectrum and any power absorption by the tip surface due to any foreign particle presence (dusts, submicron particles, etc.) was assumed negligible. It was found that the amount of power input on the fiber entrance region tip surface of the eight-fiber design decreased by 96%, from 4.6 to 0.2 W, after the use of an infrared filter [15]. See also Figs 8a and 9a.

Convection

Effect of air-cooling was studied for v_∞=5, 10 and 15 m s^{-1} with v_∞=5 m s^{-1} as a reference value. Heat transfer interactions on the entrance region of the fiber and flat-plate approximation of the entrance region tip surface are shown in Fig. 4.

The convective heat loss off the fiber entrance region tip surface was found [21] from

$$\overline{Nu}_{tip}=0.664\mathrm{Re}_{L_c}^{1/2}\mathrm{Pr}^{1/3}$$
$$(10^3<\mathrm{Re}_{L_c}<5\cdot10^5,\ \mathrm{Pr}>0.5) \quad (1)$$

where $\overline{Nu}_{tip}$ is the Nusselt number on the fiber tip surface (dimensionless), Re_{L_c} is the Reynolds number (dimensionless), $\mathrm{Re}_{L_c}=(v_\infty L_c)/\upsilon$, v_∞ is the air average velocity (m s^{-1}), L_c is a characteristic length (m), and υ is the air kinematic viscosity (m^2 s^{-1}). In Eq. (1), Pr is the Prandtl number (dimensionless), Pr=υ/α, α is the air thermal diffusivity (m^2 s^{-1}). The convective heat loss off the fiber lateral surface was found [21] from

$$\overline{Nu}_{lat}=0.3+\frac{0.62\mathrm{Re}_d^{1/2}\mathrm{Pr}^{1/3}}{\left[1+\left(\frac{0.4}{\mathrm{Pr}}\right)^{2/3}\right]^{1/4}} \quad (\mathrm{Re}_d<10^4,\ \mathrm{Pr}>0.5) \quad (2)$$

where $\overline{Nu}_{lat}$ is the Nusselt number on the fiber lateral surface (dimensionless), and d is the fiber clad diameter. The tip surface forced-convection heat transfer coefficient, average over L_s, was found

$$\bar{h}_{tip}=\frac{k}{L_c}\overline{Nu}_{tip} \quad (3)$$

Similarly, the lateral surface forced-convection heat transfer coefficient, average over d was

$$\bar{h}_{lat}=\frac{k}{d}\overline{Nu}_{lat} \quad (4)$$

where k is the air thermal conductivity (W m^{-1} K^{-1}). In Eqs (1)–(4), the core and clad materials physical properties, k, ρ, c_p, υ and α, were calculated at the bulk (film) temperature, an average of the surface (T_s) and ambient (T_∞) temperatures. For a constant T_∞ (as is the case in the paper), Eqs (3) and (4) became solely T_s-dependent.

Radiation

T-value of the fiber entrance region tip surface over the visible spectrum was about 96–97% with almost 0% *A*-value assuming no absorption by dusts or sub-micron particles and after taking into account

Table 1 Thermal, physical and optical properties for the fiber core and clad materials

Section	Polymer	Radius/mm	Refractive index/-	Melting point/°C	Temperature for TD/°C
Core	PMA	6.3	1.498	>250	60
Clad	Teflon-FEP	6.75	1.35	264	not applicable

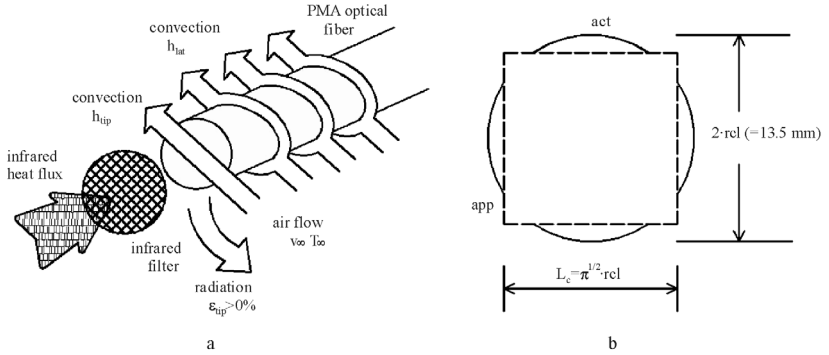

Fig. 4 a – Thermal interactions on the fiber entrance region (L_s=5 cm), b – Flat-plate approximation: act is the actual and app is the approximate cross-sectional area of the tip surface

3–4% Fresnel reflection. *T*-value over the infrared spectrum, however, was lower than this value leading to a substantial *A*-value over the infrared spectrum. With a selective coating (ε=0.6 and ε=0.8) of the fiber entrance region tip surface, the radiative heat transfer followed the Stefan–Boltzmann law [17]. The radiative heat transfer from the lateral surface of the fiber was not taken into account due to low intensity of the refracted rays into the clad and low *A*-value of the fiber over the optical spectrum [1].

Heat generation

The heat generation on the fiber entrance region was found from the difference between input and output power [6] and relating the output and input power through exponential decay-law

$$\dot{Q}_g(z)=\frac{P_{in}\{1-\exp(-\alpha_a z)\}}{\pi r_{co}^2 L_s} \quad (W\ m^{-3}) \qquad (5)$$

where $\dot{Q}_g(z)$ is the amount of heat generation (W m^{-3}) upto distance z (cm) from the fiber entrance region tip, P_{in} (W) and α_a (cm^{-1}) are the total input power and fiber average loss coefficient over the ultraviolet and visible spectrums, respectively, r_{co} is the fiber core radius (r_{co}=6.3 mm), and L_s is the length of the entrance region (L_s=5 cm).

The optical loss of the 3M optical fiber measured with a 350 W Sumitomo LBM 130H illuminator (numerical aperture, *NA*=0.4) is shown in Fig. 5. In the cut-back method, ratio of the light transmission measurements before and after cutting 1 m of the fiber was used with Eq. (5) to find α_a (m^{-1}) of the fiber.

ANSYS simulation

A finite element equation system was solved on each node of an element on the meshed structure of the fiber. The structure was comprised of solid 90 type elements each with 20 nodes, and an approximate axial length of 3 mm. The simulations implemented Jacobi conjugate gradient (JCG) iterative solver with a 0.01% convergence criterion. In the JCG iterative solver, vector {*u*} of unknown node temperatures ($T_{i,j,k}$'s) in the form [K]{*u*}={F} was solved with the global matrix [K] and load vector {F} after pre-conditioning of the global matrix for a user-specified initial condition. The {F} vector incorporated the terms for the boundary condition, temperature independent interactions such as heat generation and interactions with ambient air. More details on the JCG iteration method can be found [16].

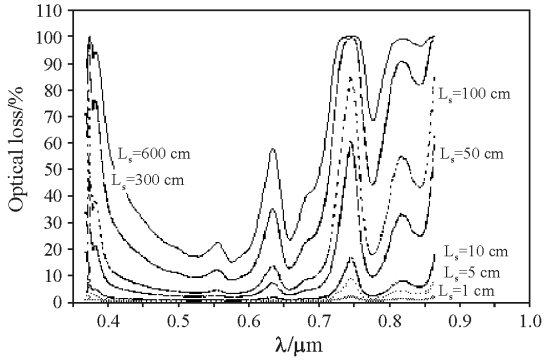

Fig. 5 PMA-core fiber optical loss with different length of the fiber (Courtesy of 3M: Published with permission)

Results and discussion

A deformed fiber entrance region is shown in Fig. 6 for the eight-fiber system from the experimental results [11]; δ is the penetration depth. It was found that first 6.5 mm of the fiber has degraded (melted) after exposition to sunlight for almost 3 h.

The experimental results are shown in Fig. 7 for the fresnel lens design with different methods of filtering [22]. It was found with a hot mirror that, first 4.0 mm of the fiber was melted after exposure to sunlight for about 20 s (Fig. 7a); it was found (Fig. 7b) with an infrared filter and same exposure time that first 4.8 mm of the fiber was deformed. With the use

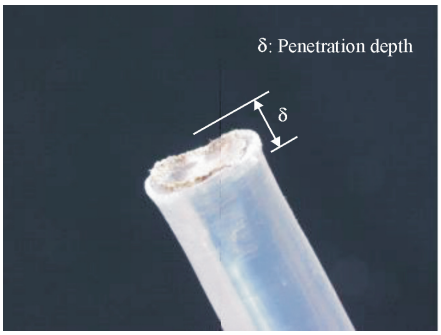

Fig. 6 Deformed shape of the fiber entrance region for the eight-fiber design, δ_{exp}~6.5 mm

of both a hot mirror and an infrared filter, the fiber core was found to have expanded about 1.6 mm after 2 h of exposure (Fig. 7c). The experimental results in Figs 7a and b showed agreement with the *T*-values of the infrared filter and hot mirror in Fig. 3b calculated 5.2 and 4.5%, respectively.

Results of the simulations were shown in Figs 8–10 for the eight-fiber design: Effect of prolonged exposition to the solar thermal radiation on the fiber entrance region temperature distribution was given in Fig. 8a, which compared with the experimental result of Fig. 6. From this figure, with ν_∞=5 m s^{-1} and τ_s=3 h (τ_s is the simulation time), a maximum temperature on the tip surface (T_{max}) 606.9°C was found. Temperature along the fiber axis was found, however, to decrease to 60°C after first 8.2 mm of the entrance region; therefore, use of some preventive measures was necessary to protect the fiber. The simulated lumen value of 7900 [15] was found to be within +5.3% of the experimentally measured value of 7500.

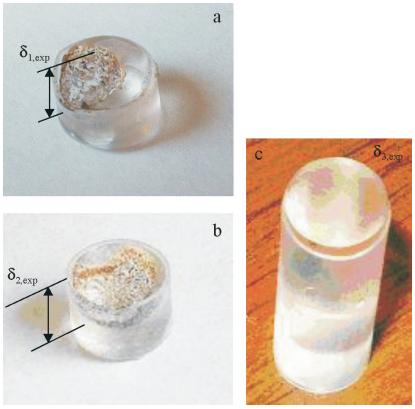

Fig. 7 Deformed shape of the fiber entrance region for the fresnel lens design. Simulation results given in parentheses. a – With a hot mirror, $\delta_{1,exp}$~4.0 mm, (T_{max}=270.9°C, δ_1=6.0 mm and τ_s=20 s). b – With an infrared filter, $\delta_{2,exp}$~4.8 mm, (T_{max}=252.3°C, δ_2=6.7 mm and τ_s=20 s). c – With a hot mirror and an infrared filter, $\delta_{3,exp}$~1.6 mm, (T_{max}=54.6°C, δ_3=not accessable and τ_s=2 h)

Effect of forced air-cooling on the fiber radial and axial temperature distribution is shown in Fig. 8b. From this figure, T_{max}=349.9°C was obtained. It was found that T_{max} with ν_∞=15 m s^{-1} and τ_s=20 s reduced by 73.6°C compared to ν_∞=5 m s^{-1}. Temperature along the fiber axial direction decreased to 60°C, however, after first 0.7 mm of the fiber.

It was obtained from Fig. 9a T_{max}>60°C, which gave a reduction of 363.5°C compared to the case with no infrared filter, with ν_∞=5 m s^{-1} and τ_s=5 min. This case in Fig. 9a was an improvement over no measurement and air-cooling cases, Figs 8a and b, respectively. The fiber entrance region, however, was prone to TD beyond τ_s=5 min. The results of the glass rod attachment to the fiber entrance region were shown in Fig. 9b. It was noted T_{max}<60°C after first 15-mm-long section of the glass rod. Beyond τ_s=30 min, temperature distribution on the entrance region reached a steady state.

Effect of using a lowered ambient temperature is shown in Fig. 10a. It was found, T_{max}=414.1°C, which was higher compared to the simulation result of Fig. 8b (case with an air-cooling). The axial temperature decreased to 60°C, however, after first 0.8 mm of the entrance region. Thus, a decreased ambient temperature (0 or –5°C) was evidenced not to be an effective way in protecting the fiber. Effect of selective-coating the tip surface (ε=80%) on the fiber entrance region temperature was shown in Fig. 10b. T_{max}=331.8°C was obtained, which was 18.1°C lower than the case in Fig. 8b. The difference between T_{max} values for ε=60 and ε=80% was found to be +17.2°C; the axial temperature decreased to 60°C after first 1.8 mm of the fiber entrance region.

In the simulations, $\dot{Q}_g$ (L_s) inside the PMA-core of the eight-fiber design were 25503 W m^{-3} (Figs 8a, b, 10a and b), 18767 W m^{-3} (Fig. 9a), and 19911 W m^{-3} inside the glass rod and 25503 W m^{-3} inside the PMA-core (Fig. 9b). From the simulations, it was found that the heat flux vector on the lateral surface of the fiber has directed outward with a magnitude decreasing along the axial direction indicating a large heat loss from the first few mm of the fiber. Also, temperature gradient inside the fiber core due to the input heat flux was steeper in the radial direction than it was in the axial direction. That is, for a cross-section of the fiber, the nodes of an element observed higher temperature in the radial direction compared to the nodes of the same element in the axial direction downstream of the fiber.

Table 2 lists the summary of the FEA results for the eight-fiber design: it was found from the simulation results that attachment of a quartz glass rod to the fiber entrance region will keep T_{max}<60°C. The light loss due to refraction from the glass lateral surface into the surroundings and the glass-fiber interface

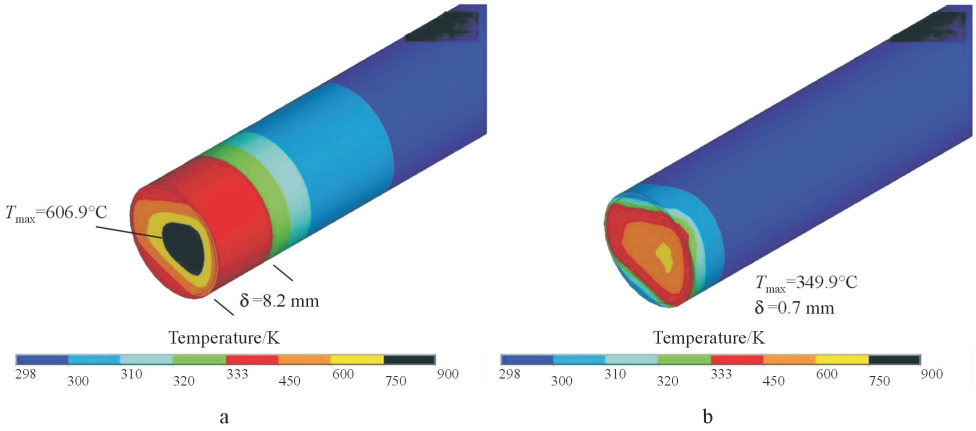

Fig. 8 Entrance region radial and axial temperature distribution: a – Effect of no preventive measure, ν_∞=5 m s^{-1}, T_∞=25°C and τ_s=3 h. b – Effect of air-cooling, ν_∞=15 m s^{-1}, T_∞=25°C and τ_s=20 s

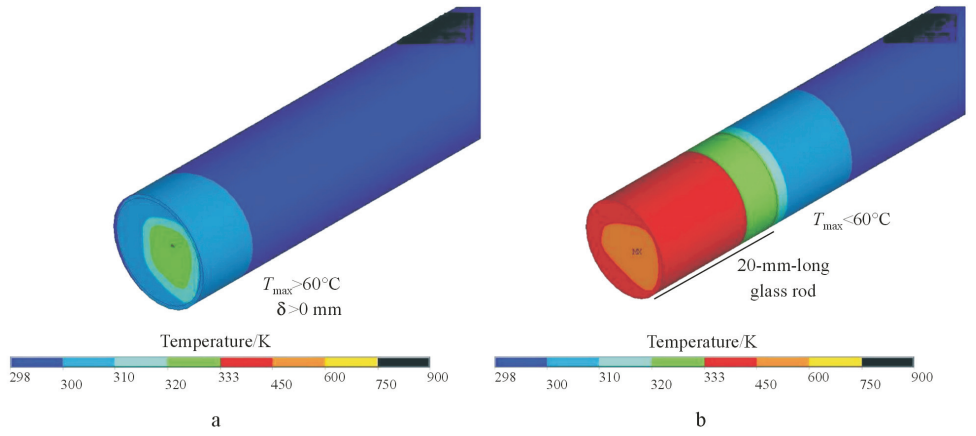

Fig. 9 a – Effect of infrared filter, ν_∞=5 m s^{-1}, T_∞=25°C and τ_s=5 min. b – Effect of 20-mm-long glass rod attachment, ν_∞=5 m s^{-1}, T_∞=25°C and τ_s=30 min

were estimated 3%. Infrared filter use alone can reduce the light input over the visible spectrum by about 14% (Fig. 3b). The use of a glass rod, therefore, in place of an infrared filter results in about 8.1% less light loss. Table 3 results for the fresnel lens design show that δ-value increases with the amount of heat flux on the entrance region tip surface.

We note for the future experimental studies of the present simulations: the weather condition affects the standard atmosphere, mechanical or electrical inaccuracy of the two-axis tracking system may cause deviation of the solar tracker from the zenith (polar) angle, focal points of the two solar collector designs can be distorted due to surface irregularities of the primary and secondary mirrors and fresnel lens, and surface roughness of optical elements may result in directive or diffuse scattering of the incident rays.

Table 2 FEA results: eight-fiber design

Method	Preventive measure	τ_s/s	T_{max}/°C	δ/mm
1	air-cooling	20	349.9	0.7
2	infrared filter	300 (=5 min)	>60	>0
3	glass rod	1800 (=30 min)	<60	0
4	lower ambient temperature	20	414.1	0.8
5	selective coating	20	331.8	1.8
6	none[1]	10800 (=3 h)	606.9	8.2

[1]case in Fig. 8a

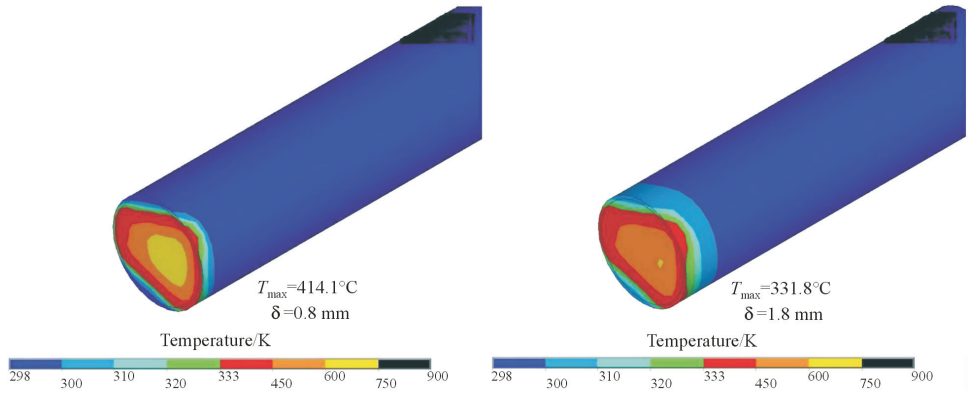

Fig. 10 a – Effect of lower ambient temperature, ν_∞=5 m s^{-1}, T_∞=–5°C and τ_s=20 s. b – Effect of selective coating, ν_∞=5 m s^{-1}, T_∞=25°C, ε=80% and τ_s=20 s

Table 3 FEA results: Fresnel lens design

Method	Preventive measure	τ_s/s	T_{max}/°C	δ/mm
1	infrared filter	20	252.3	6.7
2	hot mirror	20	207.9	6.0
3	infrared filter and hot mirror	7200 (=2 h)	54.6	*

*not assessable

Conclusions

A 3-D thermal analysis of a PMA optical fiber was performed in order to investigate ways to prevent TD of the fiber. An estimated temperature range on the fiber entrance region was given from the simulations for the two solar collector designs: eight-fiber and fresnel lens.

From the results of the simulations, a 20-mm-long glass rod was found to effectively protect the optical fiber of eight-fiber design. This preventive method was selected for a fiber entrance region tip surface temperature, T_{max}<60°C. In terms of ease and cost of application, the use of a glass rod was also favorable compared to the other solutions. The glass rod resulted in less optical loss (light) compared to the infrared filter. In fresnel lens design, the use of a glass rod, an infrared filter, and a hot mirror was found to be effective in protecting the fiber entrance region.

The simulation results showed that most-to-least effective methods of filtering in eight-fiber design were the applications of glass rod, hot mirror, infrared filter, selective coating, air-cooling, and lower ambient temperature. Selective coating of the fiber entrance region tip surface showed promise causing some tip surface cooling, however, depth of penetration remained an issue. We noted that δ was proportional to the power input on the fiber tip surface as well as type of heat transfer interactions taking place on the entrance region surface. For fresnel lens design, most-to-least effective methods of filtering, were found to be the applications of glass rod and infrared filter and hot mirror, infrared filter and hot mirror, hot mirror, and infrared filter.

We compared the simulation results with experiments on the deformed entrance region of the two experimental designs. The simulated values for δ were higher compared to the experimental results on these designs, which was attributed to the actual (smaller) amount of solar infrared power absorbed by the tip surface. This was due to that some of the absorbed power by the surface thermally radiated into the surroundings. In a future study, temperature distribution of the fiber entrance region can be found experimentally. The optical light loss due to application of the glass rod attachment needs to be quantified.

Acknowledgements

Support of the National Energy Technology Laboratory (NETL) through the United States Department of Energy (DOE) is acknowledged (Cooperative Agreement: DE-FC26-01NT41164). The authors gratefully acknowledge the ORNL for providing information on the deformed fiber of the eight-fiber design experiments. The authors also thank graduate students Jeanette Kretschmer and Hugh Currin in providing the experimental results of the fresnel lens design.

References

1 3M Company, http://www.3m.com/US/.
2 W. J. Cassarly and J. M. Davenport, Advances in Fiber Optics: Fiber Applications Move into the Mainstream, Proc. of the 8th International Symposium on the Science and Technology of Light Sources, Greifswald, Germany 1998.
3 J. Zubia and J. Arrue, Opt. Fiber Tech., 7 (2001) 101.
4 M. Tekelioglu and B. D. Wood, Appl. Opt., 44 (2005) 2318.
5 O. V. Kolninov, I. P. Shelukhov, E. R. Klinshpont, Z. N. Lavrova, A. M. Baran and V. M. Levin, Rad. Phys. Chem., 46 (1995) 843.
6 Y. Takezawa, N. Taketani, S. Tanno and S. Ohara, J. Polym. Sci. B, 30 (1992) 879.
7 V. Alvarez, E. Rodriguez and A. Vázquez, J. Therm. Anal. Cal., 85 (2006) 383.
8 H. Nagata, Opt. Fiber Tech., 6 (2000) 192.
9 Y. Takezawa, S. Tanno, N. Taketani, S. Ohara and H. Asano, J. Appl. Polym. Sci., 42 (1991) 2811.
10 S. M. Dakka, J. Therm. Anal. Cal., 73 (2003) 17.
11 Oak Ridge National Laboratory (ORNL), Photonics and Transportation Systems, Oak Ridge, TN, http://www.ornl.gov.
12 M. S. Rea, IESNA Lighting Handbook: Reference and Application, 9th Ed., Illumination Engineering Society of North America, (2000) (1-2)–(1-3).
13 O. A. Jaramillo, J. A. del Rio and G. Huelsz, J. Phys. D, 32 (1999) 1000.
14 SMARTS v2.9, Fortran code: Terrestrial direct normal solar spectral irradiance for AM=1.5, http://homepage.mac.com/smarts2.
15 TracePro, Lambda Research Corporation, Littleton, MA, http://www.lambdares.com.
16 ANSYS v6.1, http://www.ansys.com.
17 M. F. Modest, Radiative Heat Transfer, McGraw-Hill, (1993), pp. 7, 88.
18 J. Brandrup and E. H. Immergut, Polymer Handbook, 3rd Ed., John Wiley and Sons, (1989) v/77–v/79.
19 DuPont, Product and Properties Handbook, Teflon FEP (FEP 100), DuPont, (1998), p. 3.
20 N. P. Bansal and R. H. Doremus, Handbook of Glass Properties, Academic Press, (1986), pp. 11, 18 and 19.
21 A. F. Mills, Heat Transfer, 2nd Ed., Prentice Hall, (1999) pp. 313–319.
22 Energy Systems Laboratory, University of Nevada, Reno, NV 89557, USA, www.energy.unr.edu.

Received: December 28, 2005
Accepted: October 10, 2006
OnlineFirst: August 11, 2006

DOI: 10.1007/s10973-005-7493-y